

# Implementation of controllable universal unital optical channels

A. Shaham, T. Karni, and H. S. Eisenberg

*Racah Institute of Physics, Hebrew University of Jerusalem, Jerusalem 91904, Israel*

We show that a configuration of four birefringent crystals and wave-plates can emulate almost any arbitrary unital channel for polarization qubits encoded in single photons, where the channel settings are controlled by the wave-plate angles. The scheme is applied to a single spatial mode and its operation is independent of the wavelength and the fine temporal properties of the input light. We implemented the scheme and demonstrated its operation by applying a dephasing environment to classical and quantum single-photon states with different temporal properties. The applied process was characterized by a quantum process tomography procedure, and a high fidelity to the theory was observed.

PACS numbers: 03.65.Yz, 42.25.Ja, 42.50.Lc

## I. INTRODUCTION

The wave-like nature of a quantum system is manifested by the existence of a well defined phase between its components. When the system is isolated, this phase is well defined. However, when the system interacts with its surrounding, the uncertainty of the phase may increase in a process called 'dephasing' [1]. When quantum information is encoded in the phase, dephasing processes are interpreted as an addition of noise to the stored information. As a result, quantum information protocols that rely on the certainty of the phase may slow down, and their success may be hindered (see for example [2]).

Dephasing processes belong to the family of unital channels, which is a special class of decohering processes. A general decohering processes reduces the information that is stored in a quantum state, where a unital channel also preserves the average of the input state. Thus, unital channels are connected with interactions that do not include an energy dissipation from the state to its surroundings. Dephasing channels are perhaps the most common type of the unital channel class since they occur naturally in atomic and solid state quantum systems (where they are commonly characterized using the  $T_2$  decoherence time scale). In general, photonic implementations of quantum systems are more immune to decohering processes, including dephasing, since they only weakly interact with the environment. Thus, they serve as an appealing candidate in a variety of quantum information schemes [3]. The noise robustness of single photons also makes them suitable for studying decohering processes: transmitting photons through a channel that successfully induces a certain type of decohering process will not be accompanied by other types of decoherence to the photons. Hence, photons are suitable for the demonstration of the effects of different types of decohering processes on quantum systems and protocols.

In this work, we study a realization of unital channels that are applied to quantum bits (qubits) encoded in the polarization of single photons. Previously, different types of unital channels were implemented in several ways. Some works investigated the implementation of a general unital channel while other works implemented a specific channel type of the unital class, which mainly was a dephasing channel: general unital channels which were

applied on single photons where implemented using scattering from different elements [4]. Scrambling schemes that used Pockels cells [5], liquid crystals [6], or mechanical stress on optical fibers [7] were also used to construct different types of unital channels. Concentrating in dephasing schemes, a channel that completely erases the polarization phase of the photons was implemented using a single birefringent crystal [8]. Control over the dephasing level of such a channel was achieved by changing the birefringent crystal length [9, 10]. Dephasing processes could also be emulated using scrambling schemes that use wave-plates [11] or liquid crystals [12]. Another method to implement a controllable dephasing channel is to couple between the polarization and two different spatial modes via a Sagnac interferometer [13] or a polarizing tunable beam displacer [14]. Here, we study a controllable scheme that is composed of four birefringent crystals and wave-plates [15]. Previously, this scheme was only used to implement an isotropic depolarizing channel. Using a numeric search we now show that the four crystal scheme can emulate almost every arbitrary unital channel. We demonstrate the scheme operation by applying it as a dephasing channel on classical and quantum single-photon wave-packets. The measured processes are characterized using a quantum process tomography (QPT) procedure [16] and present a high fidelity to dephasing processes. Unlike dephasing schemes that are composed of one or more birefringent crystals in a fixed orientation, the four crystal configuration has the advantage that its dephasing magnitude is known in advance and is not affected by the details of the temporal structure, such as the coherence time of the initial photonic wave-packet. This property was verified by applying the dephasing scheme to two photonic states that differ in their temporal properties. As expected, the two photonic states experienced the same dephasing magnitude and agreed well with the theoretical prediction.

The structure of this article is as follows: in Sec. 2 we give a theoretical background on dephasing channels and their representations. The experimental setup for the generation and detection of single-photon states is presented in Sec. 3. Section 4 is dedicated to a theoretical study of the four birefringent crystal scheme, and for the demonstration of its operation as a dephasing channel for two photonic qubit wave-packets that differ in their coherence time. We summarize the results in Sec. 5. A complementary study of the temporal differences between the two photonic wave-packets that was performed using a Soleil-Babinet Compensator (SBC) is presented in the appendix.

## II. THEORETICAL BACKGROUND

The state of a polarization qubit can be described either by the density matrix  $\hat{\rho}$ , or by a point in the Poincaré sphere representation. The Cartesian coordinates of this point are the Stokes parameters  $\{S_1, S_2, S_3\}$ , where  $S_0 \equiv 1$ .  $S_1$  represents the linear horizontal and vertical polarizations  $|h\rangle$  and  $|v\rangle$ ,  $S_2$  represents the linear diagonal polarizations  $|p\rangle = (|h\rangle + |v\rangle)/\sqrt{2}$ , and  $|m\rangle = (-|h\rangle + |v\rangle)/\sqrt{2}$ , and  $S_3$  corresponds to the circular polarizations  $|r\rangle = (|h\rangle + i|v\rangle)/\sqrt{2}$  and  $|l\rangle = (|h\rangle - i|v\rangle)/\sqrt{2}$ . Points inside the Poincaré sphere represent partially polarized states.

Consider an arbitrary quantum channel  $\mathcal{E}$  that acts on a single-qubit state  $\hat{\rho}$ .  $\mathcal{E}$  is complete positive and linear. It can be represented as the mapping of the surface of the Poincaré sphere onto an ellipsoid which is contained within the sphere. The operation of  $\mathcal{E}$  can also

be described using the elements of the process matrix  $\chi$

$$\mathcal{E}(\hat{\rho}) = \sum_{m,n} \chi_{mn} \sigma_m \hat{\rho} \sigma_n^\dagger, \quad (1)$$

which is presented here in the basis of the identity matrix  $\sigma_0$ , and the Pauli matrices  $\{\sigma_1, \sigma_2, \sigma_3\}$ .  $\chi$  is positive, Hermitian, and satisfies  $\text{Tr}(\chi) = 1$  (i.e., the channel is lossless). Channels that obey  $\mathcal{E}(\hat{I}) = \hat{I}$  (mapping the maximally depolarized state at the origin) belong to the unital channel class. In the Poincaré sphere picture, unital channels are the case where the mapped ellipsoid and the sphere are concentric. Dephasing channels are a special case where the process can be written as

$$\mathcal{E}(\hat{\rho}) = (1 - P)\hat{\rho} + P\sigma_3\hat{\rho}\sigma_3. \quad (2)$$

They belong to the class of unital channels, and are characterized by the probability  $P$  to obtain a change in the phase of the original state. A process matrix  $\chi$  can describe a dephasing process if it has two eigenvalues that equal zero. Denote the highest eigenvalue of this  $\chi$  by  $\chi_0$ , the probability  $P$  of the corresponding dephasing process is:

$$P = 1 - \chi_0. \quad (3)$$

In order to implement a controllable dephasing channel that can vary from no dephasing to a complete dephasing it is sufficient to show that value of  $P$  can have any value in the range of  $\{0, 0.5\}$ . This is because dephasing channels with higher  $P$  values can be represented as a combination of dephasing channels with  $P$  that lies in the above mentioned range, and another deterministic bit-flip channel with a probability of 100% that can easily be built. It is clear from Eqs. (2) and (3) that in the  $\chi$  matrix representation it is sufficient to show that a fully controllable dephasing channel is obtained if the highest eigenvalue  $\chi_0$  can have any value in the range of  $\{0.5, 1\}$ , and the two lowest eigenvalues of  $\chi$  remain zero for any  $\chi_0$  settings.

A useful representation of unital single-qubit quantum processes is the tetrahedron representation: The Choi-Jamiołkowski isomorphism between complete-positive linear maps and quantum states connects between the process matrix of a single-qubit channel and the density operator of a two-qubit state [17]. Thus, we can represent the 4-dimensional (4D)  $\chi$  matrix of a single-qubit unital channel via the representation of the corresponding class of two-qubit states [18]

$$\chi = \frac{1}{4} \left( I \otimes I + \sum_{m,n=1}^3 D_{mn} \sigma_m \otimes \sigma_n \right). \quad (4)$$

Here,  $D$  is a  $3 \times 3$  real matrix, that epitomizes all the channel parameters. Ignoring rotations, the process of the channel can be geometrically represented by the coordinate vector  $\vec{D} = \{D_1, D_2, D_3\}$ , which is composed of the eigenvalues of  $D$ . The complete positivity of the process is equivalent to the requirements that

$$|D_i \pm D_j| \leq |1 \pm D_k|, \quad (5)$$

where  $i \neq j \neq k$  [19]. Equation (5) dictates that all allowed  $\vec{D}$  vectors, when drawn in a cartesian 3D coordinate systems, span the volume of a tetrahedron. The values of  $\{D_1, D_2, D_3\}$  are related to the eigenvalues of the corresponding  $\chi$  ( $\chi_0, \chi_1, \chi_2, \chi_3$ ) by

$$D_i = \chi_0 + \chi_i - \chi_j - \chi_k, \quad (6)$$

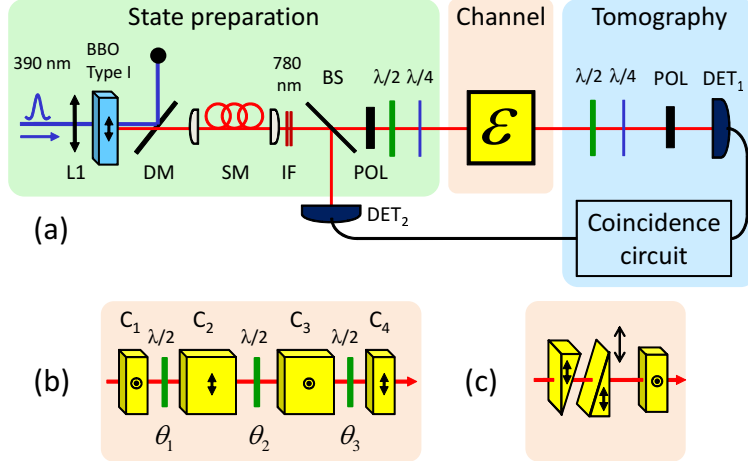


FIG. 1. (a) The experimental setup for the characterization of single-qubit channels. Photon pairs are generated in the BBO crystal, which is located after a lens (L1). The down-converted signal is filtered by passing through a dichroic mirror (DM), a single-mode fiber (SM) and an interference bandpass filter (IF). The photon pairs are split into two ports using a BS, where single-photon detectors ( $\text{DET}_1$ ,  $\text{DET}_2$ ) are located at the end of each port. The investigated channel ( $\mathcal{E}$ ) is applied only on photons that emerge from one of the ports. The initial polarization state of these photons is determined using a polarizer (POL), a HWP ( $\lambda/2$ ) and a QWP ( $\lambda/4$ ), and their final polarization state is measured using a HWP, a QWP and a polarizer that are placed after the channel. (b) The four-crystal scheme, composed of four perpendicularly-oriented calcite crystals and three HWPs. The thickness of the two outer (inner) crystals is 1 mm (2 mm). (c) A Soleil-Babinet compensator, composed of two translatable quartz wedges and another rectangular fixed quartz crystal (see details in the appendix).

where  $i \neq j \neq k \neq 0$  [19]. It can be shown that the eigenvalues of  $D$  are equal to the lengths of the three primary radii of the mapped ellipsoid in the Poincaré sphere representation of the process. In the tetrahedron representation, the identity process ( $\mathcal{E}(\hat{\rho}) = \hat{\rho}$ ) is represented by the  $\{1, 1, 1\}$  vertex of the tetrahedron, and any arbitrary dephasing channel with a corresponding probability  $P$  is represented by a point that lies on the tetrahedron edge of  $\vec{D} = \{1 - 2P, 1 - 2P, 1\}$ .

### III. EXPERIMENTAL SETUP

The experimental setup which was used to characterize the implementation of the dephasing channel is presented in Fig. 1(a). A pulsed 390 nm pump laser is focused onto a 1 mm thick type-I  $\beta - \text{BaB}_2\text{O}_4$  (BBO) crystal. Photon pairs are collinearly generated via the process of spontaneous parametric down conversion. After the BBO crystal, the down converted signal is separated from the 390 nm pump beam by passing through a dichroic mirror. Spatial and temporal filtering of the 780 nm photon pairs is achieved by sending the photon pairs through a single-mode fiber, and a 5 nm interference bandpass filter, respectively. Then, the two photons are split probabilistically using a beam splitter (BS), where one photon is sent directly to a detector, and the second photon is directed to the investigated single-qubit channel. The initial polarization state of the photon that is sent

to the channel is set using a polarizer, a half- and a quarter-wave plates (HWP and QWP). After the channel, the output polarization state is measured using a standard quantum state tomography (QST) procedure [20]: the photon passes a QWP, a HWP and a polarizer before being coupled to the detector.

We performed a complete QPT for every channel setting by characterizing the channel effect on  $|h\rangle$ ,  $|v\rangle$ ,  $|p\rangle$ , and  $|r\rangle$  polarization states [16]. When only the counts of photons that pass through the dephasing channel (counts from  $\text{DET}_1$ ) are considered, the channel effect on a classical single-photon state (i.e., a weak signal photonic state that has the thermal statistics of the down conversion process) is measured. When the detection of the photon that experiences the dephasing noise is also conditioned in the detection of another photon that does not pass through the channel (i.e., coincidence counts from both  $\text{DET}_1$  and  $\text{DET}_2$  are counted), the channel effect on quantum single-photon states that have different temporal coherence properties is investigated. The classical and the quantum single-photon wave-packet states differ in their temporal properties, as the quantum wave-packet has a longer coherence time than classical wave-packet. In order to verify this difference, we studied the effect of a dephasing scheme which is composed of a SBC (see Fig. 1(c)) on the classical and the quantum wave-packets [21]. The dephasing results which clearly demonstrate the difference between the two wave-packet types are presented in the appendix. The typical count rate of single counts (photon hits in one detector disregarding the other one) was  $\sim 20,000$  Hz, and the rate of the coincidence counts was  $\sim 1000$  Hz. Single counts were considered and analyzed after the subtraction of a stray light signal noise (background counts were estimated to be in the order of 2000 Hz). As for the coincidence counts, no subtraction was required since the stray light signal noise was negligible. Errors were calculated using a maximal likelihood procedure and Monte Carlo simulations, assuming Poissonian noise for the photon counts [22, 23].

#### IV. FOUR-BIREFRINGENT CRYSTAL SCHEME AS A DEPHASING CHANNEL

In order to apply decoherence to polarization qubits, one should entangle the polarization degree of freedom (DOF) with extra DOFs that are not going to be measured, effectively increasing the dimension of the state Hilbert space. Ignoring the extra DOFs, the measured density matrix of the polarization DOF is obtained after tracing out these extra DOFs. Such a coupling between the polarization and additional temporal DOFs of the wave-packet can be achieved using a depolarizer that is composed of birefringent crystals and wave-plates in between them [8, 24]. Consider a polarized wave-packet of photons with a coherence time  $\tau$  that passes through such a depolarizer. A crystal with a length  $L$  induces a temporal delay  $t = L \frac{\Delta n}{c}$  between the fast and the slow polarization modes, where  $\Delta n$  is the birefringent index difference and  $c$  is the speed of light. We require that all crystals are sufficiently long such that the temporal delay between different polarization modes of the output states is much larger than the coherence time of the photons  $\tau$ :

$$L \frac{\Delta n}{c} \gg \tau. \quad (7)$$

After the passage through the depolarizer, the wave-packet occupies a discrete number of temporal modes. These modes do not overlap in between them, and every different temporal mode is fully polarized by itself. The photon-detectors are insensitive to small

temporal differences between the different modes and do not record them. As a result, the temporal DOFs of the photonic state are traced out and decohered mixed states are detected. The mixture level of the detected state depends only on the occupation of each temporal mode and is a function of the input polarization state, and the relative angle between the polarization state and the primary axes of the crystal [24]. It does not depend on the temporal shape of the discrete modes which is inherited from the input temporal shape and properties. Thus, as long as the relation of Eq. (7) is kept, the decoherence process that is induced by such a depolarizing scheme is the same regardless of the exact temporal shape of the photonic wave-packet. Turning the wave-plates between the crystals affects the relative occupation of each different temporal mode and controls the decoherence properties that are to be measured.

We study a decohering scheme that is composed of four fixed calcite crystals ( $C_1, \dots, C_4$ ), and three tunable HWPs ( $\theta_1, \theta_2, \theta_3$ ) in between them (see Fig. 1(b)) [15]. The length of  $C_2$  and  $C_3$  is 2 mm, and the length of  $C_1$  and  $C_4$  is 1 mm. The fast axes of  $C_1$  and  $C_3$ , and the slow axes of  $C_2$  and  $C_4$  are parallel, and define the zero angle of the wave-plates. This scheme couples between the polarization DOF and seven possible temporal modes: recall that a 1 mm crystal induces a time delay of  $\Delta t$  between the fast and the slow polarization modes, the maximal time delay is obtained between a polarization mode that travels through the fast axis of every crystal in the configuration, and the polarization mode that travels through the slow axis of every crystal, and equals  $(1 + 2 + 2 + 1)\Delta t = 6\Delta t$ . Polarization modes that travel through fast axis of some crystals and the slow axis of the other ones occupy all temporal modes which are the multiplications of  $\Delta t$  that lie between  $t = 0$  and  $t = 6\Delta t$ , so that seven different temporal modes are obtained (for a detailed mathematical description of the different temporal modes see also [24]). Hence, a polarization qubit that passes through this scheme resides within a 14-dimensional time-polarization Hilbert space. For photons with a wavelength of 780 nm, the temporal delay between two successive modes is  $\sim 570$  fs. The coherence time  $\tau$  of the down converted single-photon wave-packets before entering the scheme is  $\sim 180$  fs (it is mainly governed by the 5 nm interference bandpass filter). Thus, the requirement of Eq. (7) is fulfilled and the seven different temporal modes can be regarded as discrete ones.

Tuning the HWPs to different angles, different processes are induced by the scheme. The values of the different  $D_i$  parameters (Eq. (6)) that represent these processes as a function of the HWP angles are

$$D_1 = -\sin(4\theta_1) \sin(4\theta_3) \cos^2(2\theta_2) + \cos(4\theta_1) \cos(4\theta_2) \cos(4\theta_3), \quad (8)$$

$$D_2 = \sin(4\theta_2) \sin(2\theta_1 + 2\theta_3) \cos(2\theta_1) \cos(2\theta_3) - \cos^2(2\theta_2) \cos^2(2\theta_1 + 2\theta_3) - \frac{1}{2} \sin(4\theta_1) \sin(4\theta_3) \sin^2(2\theta_2), \quad (9)$$

$$D_3 = -\sin(4\theta_2) \sin(2\theta_1 + 2\theta_3) \cos(2\theta_1) \cos(2\theta_3) - \cos^2(2\theta_2) \cos^2(2\theta_1 + 2\theta_3) - \frac{1}{2} \sin(4\theta_1) \sin(4\theta_3) \sin^2(2\theta_2). \quad (10)$$

We emphasize that these values are calculated up to rotations that flip the sign of two  $D_i$  values. Cancellation of these rotations can be achieved by adding more fixed wave-plates before the crystals, or by tilting one of the crystals to change the induced birefringent phase.

Using Eqs. (8)- (10), we numerically investigated the spanned volume in the tetrahedron representation that represents all possible processes that can be emulated by this scheme. The spanned volume is shown in Fig. 2(a). The presented possible process range can be

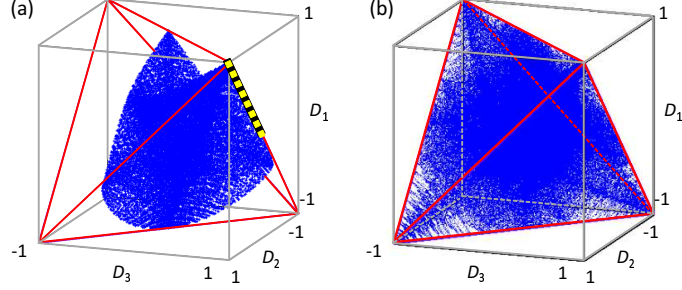


FIG. 2. Numerical investigation of the possible channels of the four-crystal scheme in the tetrahedron representation. (a) All possible channels using different orientations of the three HWPs of the four-crystal scheme. (b) All possible channels using the different orientations of the three HWPs of the four-crystal scheme, with the addition of all allowed polarization rotations. These rotations can be implemented using more wave-plates that are placed after the scheme. Points on the dashed yellow line along the edge of the tetrahedron in (a) correspond to a dephasing channel that preserves the length of  $D_3$ .

extended with the addition of polarization rotations that are described by two transformations: cyclic permutations between the three  $D_i$  values, and sign-flips of two  $D_i$  values. The extended process range is presented in Fig. 2(b). It can be seen from Fig. 2(b) that almost every complete positive unital qubit map can be implemented using the investigated four-crystal scheme.

Observing Fig. 2(a), it can be inferred that a dephasing channel can be implemented using this scheme, since the spanned volume almost covers the edges of the tetrahedron. However, a careful examination reveals that only an approximation of the dephasing channel can be implemented. It can be proved that there is no solution to Eqs. (8)-(10), that preserves the length of one of the  $D_i$  values equal to 1, while the absolute values of the two other parameters have values in the range of (0,1). Thus, points on the edges which correspond to a dephasing process are not attainable. We examined the properties of the points that are in the vicinity of the edges, and found that an approximation to the dephasing channel is obtained for the following relation between the three HWPs angles of the four-crystal scheme:

$$\theta_1 = \theta_3 = \frac{\theta_2}{2}. \quad (11)$$

Maintaining this relation, we calculated the corresponding process matrices  $\chi$  for  $0 \leq \theta_1 \leq 45^\circ$ . A plot of the eigenvalues of  $\chi$  as a function of  $\theta_1$  is presented in Fig. 3(a). One of the eigenvalues remains zero for every angle setting, and a second one is approximately zero for small  $\theta_1$  angles (see the gray area in Fig. 3(a)). The two other eigenvalues participate in the process for every angle, and intersect when  $\theta_1 \simeq 9^\circ$ . Thus, an approximation to a dephasing channel is obtained when  $\theta_1$  is in the range of  $0 \leq \theta_1 \leq 9^\circ$ , and the other two HWP angles satisfy Eq. (11).

We denote the highest eigenvalue of  $\chi$  by  $\chi_m$ . Using Eqs. (2), (3), (6), (8)-(10) and (11), the dephasing probability  $P$  that is induced by the approximated dephasing channel can be written as a function of  $\theta_1$ :

$$P = 1 - \chi_m = \frac{-3 \cos^4(4\theta_1) + 2 \cos^2(4\theta_1) + 1}{2}. \quad (12)$$

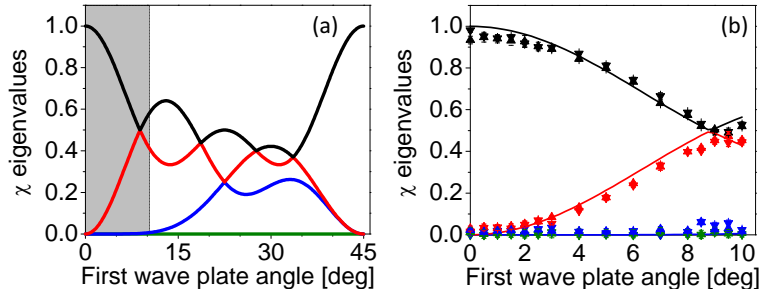


FIG. 3. Four-crystal scheme as a dephasing channel. (a) Calculated eigenvalues of the  $\chi$  matrix as a function of the first HWP angle. (b) Measured eigenvalues of the  $\chi$  matrix as a function of the first HWP angle for the dephasing range ( $0 \leq \theta_1 \leq 10^\circ$ , gray area of (a)). Eigenvalues that were reconstructed from counts of a single detector (coincidence measurements) are presented as upright triangles (upside-down triangles). Solid lines are the theoretical prediction.

In a similar manner to the definition of the fidelity between two quantum states [25], the fidelity  $F$  between two different processes can be defined as

$$F(\hat{\chi}_1, \hat{\chi}_2) = \left( \text{Tr} \left( \sqrt{\sqrt{\hat{\chi}_1} \hat{\chi}_2 \sqrt{\hat{\chi}_1}} \right) \right)^2. \quad (13)$$

Comparing between a theoretical ideal controlled dephasing channel and the theoretical prediction of the approximated dephasing processes in the range  $0 \leq \theta_1 \leq 9^\circ$  that have the same corresponding  $P$ , the minimal value of the calculated process fidelity is 99.6%. Actually, such a high value is better than the typical accuracy that is achieved in experimental realizations of such channels. It is important to mention that the induced processes are not accompanied by nontrivial rotations: defining the  $S_1$  polarization directions as the directions of primary axes of the crystals, the channel maintains the  $S_2$  value of the input light, and reduces the absolute values of  $S_1$  and  $S_3$ . It also flips the signs of the  $S_2$  and  $S_3$  parameters - a sign flip that can be compensated for by adding a fixed HWP in a zero angle before or after the channel.

Implementing the four-crystal scheme (Fig. 1(b)), we measured the processes that approximate the dephasing channel using the setup of Fig. 1(a). Figure 3(b) presents the measured eigenvalues of the  $\chi$  matrices that were reconstructed from the data of classical single-photon wave-packets, as well as those who were reconstructed from the data of quantum wave-packets (see details in the experimental setup section). The eigenvalues are presented as a function of  $\theta_1$  along with the theoretical prediction. The measured results are in good agreement with theory, and the control over the dephasing level from no dephasing ( $\theta_1 = 0$ ) to a complete dephasing ( $\theta_1 \simeq 9^\circ$ ) is achieved. As expected, no significant differences between the dephasing processes of wave-packets with different temporal properties are observed. Neglecting channel rotations, the average fidelity between the measured processes and the theoretical dephasing processes (which were calculated using Eq. (12) for the corresponding  $\theta_1$  angle) is  $97 \pm 2\%$ , both for the processes which were applied to classical and to quantum single-photon wave-packets. For light of a broader spectral bandwidth we expect to obtain even better results: such a wave-packet has a shorter coherence time and the requirement of Eq. (7) is easily fulfilled since the overlap between different temporal modes after the passage through the crystal is more negligible. Thus, Eqs. (8)-(10) more faithfully represent the decoherence of the polarization state, and a similar experiment will

show a higher fidelity to the theoretical calculation when compared to the presented classical and quantum wave-packet cases.

## V. CONCLUSIONS AND DISCUSSION

To summarize, we investigated a controllable photonic dephasing channel of a single spatial mode that is composed of four birefringent crystals and wave-plates. This configuration can emulate almost every arbitrary unitary channel. The operation of the channel as a dephasing channel was experimentally demonstrated, and was characterized using single-photon wave-packets with different coherence times. There is a high fidelity between the operation of the explored scheme and that of an ideal dephasing environment, where the dephasing rate is in agreement with the theoretical prediction. As expected, the noise probability of the four crystal scheme is known in advance and is not affected by changes in the temporal envelope of the photonic wave-packet. The presented scheme is not limited to single-photon states. It can be applied on a high-intensity classical light of a short coherence time (or a broader bandwidth), and serve as a depolarizer that emulates almost any unitary process. In the case of a wave-packet that has a longer coherence time, the birefringent crystals can be replaced by polarization maintaining birefringent fibers which act as longer birefringent crystals.

### APPENDIX: SBC AS A DEPHASING CHANNEL FOR CLASSICAL AND QUANTUM SINGLE-PHOTON WAVE-PACKETS

In order to show that the classical and quantum single-photon wave-packets differ in their fine temporal properties and that this difference affects the dephasing level that these wave-packets experience when transmitted through a common dephasing channel, we transmitted the same investigated states through a SBC dephasing scheme [21] (see Fig. 1(c) in the main text). The SBC dephasing scheme is composed of two birefringent crystal prisms with parallel optical axes, which may be followed by another birefringent rectangular crystal. The passage through the crystal prisms results in a temporal delay of  $t = L \frac{\Delta n}{c}$  between the two polarization modes (here  $L$  is the *total* optical path inside the birefringent medium). When one of the prisms is transversely translated,  $L$  is changed, and a control over the time delay  $t$  is attained. When  $t$  is comparable or larger than the initial wave-packet coherence time  $\tau$ , the temporal overlap between the two polarization modes is reduced and the phase uncertainty between the two polarizations increases (i.e., the photons experience a dephasing process). If a rectangular crystal is added to the beam path (see Fig. 1(c)), such that its optical axes are perpendicularly oriented with respect to the two prisms, the polarization modes can be temporally overlapped again and a dephasing process with a small or a zero probability is emulated.

The SBC dephasing channel was implemented using two wedge quartz crystals with a wedge angle of  $15^\circ$ , and another 9 mm rectangular quartz crystal. The chosen wedge angles of the crystals enable a time delay up to  $t \sim 380$  fs. Such a time delay is larger by almost 2 orders of magnitude than the maximal time delay that a typical Soleil-Babinet compensator can induce. As was mentioned before, the coherence time  $\tau$  of the down converted photons is  $\sim 180$  fs. As a result, we could continuously switch between different dephasing levels. For every translation setting,  $t$  was calculated using the optical path inside the birefringent

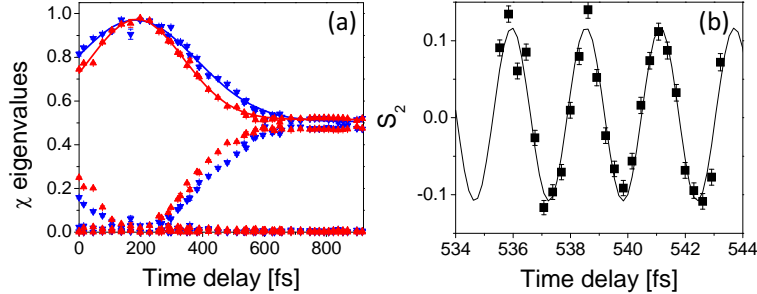


FIG. 4. (a) The eigenvalues of the  $\chi$  matrix as a function of the time delay  $t$  between the two polarization modes. Eigenvalues of process matrices that were reconstructed from counts of single detector (coincidence measurements) are presented as red upright triangles (blue upside-down triangles). Solid lines are Gaussian fits to lead the eye. (b) The oscillations of the Stokes parameter  $S_2$  as a function of the time delay between the two polarization modes. Solid line represents a sinusoidal fit.

quartz medium. We define  $t$  to be in the range of  $0 < t < \sim 380$  fs when the primary axes of the rectangular crystal are perpendicular to those of the wedge crystals. The range of  $t$  is extended up to 900 fs using different settings of the third rectangular crystal: time range of  $\sim 270$  fs  $< t < \sim 650$  fs is obtained when the rectangular crystal is omitted, and time range of  $\sim 530$  fs  $< t < \sim 920$  fs is attained when the rectangular crystal primary axes are parallel to those of the wedge crystals.

Performing a standard QPT procedure on the channel, we reconstructed the process matrix  $\chi$  for different translation settings. The eigenvalues of the reconstructed  $\chi$  matrices are presented in Fig. 4(a) as a function of the induced temporal delay  $t$ . As in the four crystal case, the processes were separately reconstructed from data of classical and quantum wave-packet states. It can be seen that both states experience a dephasing operation since for every  $t$ , two  $\chi$  eigenvalues remain close to zero. When  $t \simeq 185$  fs, the operation of the channel is very close to having no effect. The corresponding measured processes from both data sets for this temporal setting have fidelities higher than  $95 \pm 2\%$  to the no-decohering process (disregarding polarization rotations). When compared to the quantum single-photon wave-packet, it is clear from Fig. 4(a) that the classical single-photon wave-packet experiences a faster dephasing process. This demonstrates the difference between the two wave-packet states, and shows the dependence of the dephasing probability of the SBC scheme in the temporal shape of the incoming photonic state, unlike the four crystal scheme (see Fig. 3(b) in the main text).

It is worth mentioning that although the wedge angle of the channel is larger with respect to that of a typical Soleil-Babinet compensator, the SBC dephasing scheme realization can also serve as a solid and stable polarization interferometer. Figure 4(b) presents the oscillations of the  $S_2$  Stokes parameter as a function of the temporal delay. The oscillations were measured for the quantum single-photon wave-packet state, when a heavy dephasing process is applied to the photons ( $P \sim 0.45$ ). Analyzing the presented oscillations, the calculated wavelength of the photons is  $775 \pm 15$  nm, in agreement with the set value of 780 nm.

## FUNDING

We thank the Israel Science Foundation for supporting this work under Grants No. 546/10 and 793/13. We also thank the Israeli Ministry of Science and Technology for financial support through the Eshkol fellowship for A.S.

- 
- [1] M. A. Nielsen and I. L. Chuang, *Quantum Computation and Quantum Information* (Cambridge University, Cambridge, U.K., 2000).
  - [2] J. I. Cirac, A. K. Ekert, S. F. Huelga, and C. Macchiavello, “Distributed quantum computation over noisy channels,” *Phys. Rev. A* **59**(6), 4249-4254 (1999).
  - [3] J. I. O’Brien, A. Furusawa, and J. Vučković, “Photonic quantum technologies,” *Nature Photon.* **3**, 687-695 (2009).
  - [4] G. Puentes, D. Voigt, A. Aiello, and J. P. Woerdman, “Experimental observation of universality in depolarized light scattering,” *Opt. Lett.* **30**, 3216-3218 (2005).
  - [5] M. Ricci, F. De Martini, N. J. Cerf, R. Filip, J. Fiurášek, and C. Macchiavello, “Experimental purification of single qubits,” *Phys. Rev. Lett.* **93**, 170501 (2004).
  - [6] A. Chiuri, V. Rosati, G. Vallone, S. Pádua, H. Imai, S. Giacomini, C. Macchiavello, and P. Mataloni, “Experimental realization of optimal noise estimation for a general Pauli channel,” *Phys. Rev. Lett.* **107**, 253602 (2011).
  - [7] M. Karpiński, C. Radzewicz, and K. Banaszek, “Fiber-optic realization of anisotropic depolarizing quantum channels,” *J. Opt. Soc. Am. B* **25**(4), 668-673 (2008).
  - [8] P. G. Kwiat, A. J. Berglund, J. B. Altepeter, and A. G. White, “Experimental verification of decoherence-free subspaces,” *Science* **290**, 498-501 (2000).
  - [9] J.-S. Xu, C.-F. Li, X.-Y. Xu, C.-H. Shi, X.-B. Zou, and G.-C. Guo, “Experimental characterization of entanglement dynamics in noisy channels,” *Phys. Rev. Lett.* **103**, 240502 (2009).
  - [10] B.-H. Liu, L. Li, Y.-F. Huang, C.-F. Li, G.-Can Guo, E.-M. Laine, H.-P. Breuer, and J. Piilo, “Experimental control of the transition from Markovian to non-Markovian dynamics of open quantum systems” *Nature Physics* **7**, 931934 (2011).
  - [11] E. Amsalem and M. Bourennane, “Experimental four-qubit bound entanglement,” *Nature Phys.* **5**, 748-752 (2009).
  - [12] R. B. A. Adamson, L. K. Shalm, and A. M. Steinberg, “Preparation of pure and mixed polarization qubits and the direct measurement of figures of merit,” *Phys. Rev. A* **75**, 012104 (2007).
  - [13] M. P. Almeida, F. de Melo, M. Hor-Meyll, A. Salles, S. P. Walborn, P. H. S. Ribeiro, and L. Davidovich, “Environment-induced sudden death of entanglement,” *Science* **316**, 579-582 (2007).
  - [14] D. F. Urrego, J.-R. Álvarez, O. Calderón-Losada, J. Svozilík, M. Nuñez, and A. Valencia, “Implementation and characterization of a controllable dephasing channel based on coupling polarization and spatial degrees of freedom of light,” *Opt. Express* **26**, 11940-11949 (2018).
  - [15] A. Shaham and H. S. Eisenberg, “Realizing a variable isotropic depolarizer,” *Opt. Lett.* **37**(13), 2643-2645 (2012).
  - [16] I. L. Chuang and M. A. Nielsen, “Prescription for experimental determination of the dynamics of a quantum black box,” *J. Mod. Opt.* **44**(11-12), 2455-2467 (1997).

- [17] A. Jamiolkowski, "Linear transformations which preserve trace and positive semidefiniteness of operators," *Rep. Math. Phys.* **3**(4), 275-278 (1972).
- [18] M. Horodecki and R. Horodecki, "Information-theoretic aspects of inseparability of mixed states," *Phys. Rev. A* **54**(3), 1838-1843 (1996).
- [19] C. King and M. B. Ruskai, "Minimal entropy of states emerging from noisy quantum channels," *IEEE Trans. Inf. Theory* **47**(1), 192-209 (2001).
- [20] D. F. V. James, P. G. Kwiat, W. J. Munro, and A. G. White, "Measurement of qubits," *Phys. Rev. A* **64**, 052312 (2001).
- [21] D. Branning, A. L. Migdall, and A. V. Sergienko, "Simultaneous measurement of group and phase delay between two photons," *Phys. Rev. A* **62**, 063808 (2000).
- [22] J. B. Altepeter, E. R. Jeffrey, and P. G. Kwiat, "Photonic state tomography," *Adv. At. Mol. Opt. Phys.* **52**, 105-159 (2005).
- [23] A. Shaham and H. S. Eisenberg, "Quantum process tomography of single-photon quantum channels with controllable decoherence," *Phys. Scr.* **T 147**, 014029 (2012).
- [24] A. Shaham and H. S. Eisenberg, "Realizing controllable depolarization in photonic quantum-information channels," *Phys. Rev. A* **83**, 022303 (2011).
- [25] R. Jozsa, "Fidelity for mixed quantum states," *J. Mod. Opt.* **41**, 2315-2323 (1994).